AIAA JOURNAL
Vol. 48, No. 9, September 2010

Numerical Study of Wind-Tunnel Sidewall Effects on Circulation Control Airfoil Flows

Takafumi Nishino* and Karim Shariff†
NASA Ames Research Center, Moffett Field, California 94035

DOI: 10.2514/1.J050328

Two- and three-dimensional numerical simulations are performed of the flow around a circulation control airfoil (using a Coanda jet blowing over a rounded trailing edge) placed in a rectangular wind-tunnel test section. The airfoil model spans the entire tunnel and the span-to-chord ratio of the model is 3.26. The objective of this numerical study, in which we solve the compressible Reynolds-averaged Navier–Stokes equations in a time-resolved manner (but the solutions eventually converge to steady states), is to investigate the physical mechanisms of wind-tunnel sidewall effects on the flow, especially in the midspan region. The three-dimensional simulations predict that the Coanda jet flow is quasi-two-dimensional until the flow separates from the trailing edge of the airfoil; however, the spanwise ends of this Coanda jet sheet then three-dimensionally roll up on the side walls of the wind tunnel to form two large streamwise vortices downstream. Careful comparisons between the two- and three-dimensional simulations reveal that the wind-tunnel stream goes below the airfoil more in the three-dimensional cases than in the two-dimensional cases due to the presence of these two streamwise vortices downstream. This results in smaller lift and larger drag being produced at the midspan of the airfoil in the three-dimensional cases than in the two-dimensional cases.

I. Introduction

CIRCULATION control (CC) is one of the key technologies for cruise efficient short takeoff and landing aircraft, a promising candidate for the next generation of passenger aircraft proposed by NASA. The concept of CC for this application is to increase aerodynamic circulation around a wing by, for example, applying Coanda wall jet blowing over a rounded trailing edge of the wing, and thereby enhancing the lift for short-distance takeoff and landing. A general introduction to CC can be found in, e.g., [1]. While several different types of CC devices have been proposed in the past (for example, those using a rotating cylinder attached to a truncated trailing edge of a wing [2]), the present paper focuses only on those using Coanda wall jet blowing over a rounded trailing edge.

One present challenge facing the implementation of CC technologies on passenger aircraft is to improve the accuracy of flow prediction tools that can be used in practical design and optimization. Currently, those prediction tools are mostly based on Reynolds-averaged Navier–Stokes (RANS) approaches because direct numerical simulations of the Navier–Stokes equations are infeasible for most practical applications. Earlier studies have shown that the separation location of the Coanda jet flow, which is critical to the performance of CC devices, is difficult to accurately predict using existing RANS models [3–6]. Several researchers, including the present authors, have recently been performing large-eddy simulations (LES) of flow around a basic CC airfoil model [7–10], which can provide comprehensive turbulence data for the Coanda flow (not easily obtainable from wind-tunnel tests) and thus contribute to the improvement of existing RANS models. A new challenge here, however, is that these LES also need to be carefully validated against wind-tunnel tests, which are subject to wind-tunnel wall effects that cannot be directly addressed in LES (because these LES can be performed only for a rather limited portion of the wing span due to their huge computational cost). A conventional way of comparing such LES against wind-tunnel tests has been to estimate and use an angle-of-attack correction [8,11,12]; however the actual flowfield around a CC wing may be altered by the wind-tunnel walls in a more complicated manner, the physical mechanisms of which have not been investigated in detail. To sum up, better understanding the effects of wind-tunnel walls is an essential step towards making a reliable comparison between such LES and wind-tunnel tests and thus creating a comprehensive turbulent-flow database that can be used for the improvement of existing flow prediction tools (for CC devices and also for other similar flow separation problems).

A difficult issue here, however, is that we need to rely on the very same, existing prediction tools (based on RANS approaches, or possibly RANS–LES hybrid approaches such as detached-eddy simulations [13,14]) to investigate the mechanisms of wind-tunnel wall effects. An experimental study has been reported by Wood and Rogers [11] on two-dimensional (2-D) tunnel blockage effects for basic CC airfoils; however it is very difficult to study the details of three-dimensional (3-D) tunnel wall effects experimentally or analytically. The effects of 3-D wind-tunnel walls for a general three-element high-lift wing (i.e., a wing equipped with a slat and a flap) have been numerically investigated by, for example, Rogers et al. [15], who successfully performed 3-D RANS simulations using the Spalart–Allmaras (SA) model [16] on this flow configuration. For a CC wing, however, such a detailed 3-D study has not been successfully performed so far. A particular difficulty here is that steady RANS computations for a CC wing with strong Coanda jet blowing hardly converge to a physically correct steady solution. Only recently have some preliminary results been reported of 3-D RANS simulations for a CC wing placed in a wind tunnel [6]; for a stronger jet blowing case, the solutions were found to be oscillating and qualitatively incorrect, or unphysical, in the sense that the Coanda flow wrapped completely around the rounded trailing edge and back upstream along the airfoil lower surface.

In the present study, we perform 3-D compressible RANS simulations with the equations being solved in a time-resolved manner, which incur large computational costs but eventually converge to qualitatively correct, steady solutions. A fine enough spanwise grid resolution is used to examine 3-D vortical flow structures near the side walls of the wind tunnel. For the turbulence model, the two-equation shear stress transport (SST) model of Menter [17] is mainly employed and the SA model is used for comparison. The flow regime investigated is limited to subsonic and, therefore, the results might not be directly applicable to practical, high-Mach-number CC applications; however, fundamental physical insights obtained are still of great interest. It should be noted that the objective of the

Received 2 November 2009; revision received 17 March 2010; accepted for publication 24 April 2010.

*NASA Postdoctoral Program Fellow. Member AIAA.
†Research Scientist.

present study is to numerically investigate the fundamental effects of 3-D wind-tunnel walls by using qualitatively correct RANS solutions. It is *not* the objective of the present study to make a quantitative comparison with experimental results, which is an important topic for future study.

II. Geometry and Flow Conditions

Figure 1 shows the geometry of the CC airfoil model investigated in this study. This airfoil model was designed by Dr. Englar's research group at Georgia Tech Research Institute [18] and is also being tested in the BART facility at NASA Langley Research Center [19]. This two-dimensional, noncambered CC airfoil model has a semicircular trailing edge, equipped with two independent jet slots on the upper and lower sides, and two independent blowing plenums (each consisting of two chambers) inside the model. For the present study, however, the lower jet slot is not used (i.e., closed). The chord length of the airfoil c is 8.594 in., the trailing-edge radius r is 0.813 in. ($0.09463c$), and the upper jet slot height h is 0.0198 in. ($0.02433r$).

Figure 2 shows the computational domain and boundary conditions used in this study. The airfoil model, at 0 deg angle of attack, spans a rectangular wind-tunnel test section 28 in. wide and 40 in. high and is located 31.125 in. downstream from the inlet of the test section, all of which follow the configuration of the aforementioned wind-tunnel tests at NASA Langley Research Center. Note that the span-to-chord ratio of the airfoil model is 3.26. In the present numerical study, however, only half of the test section in the spanwise direction is computed with symmetric boundary conditions applied at the midspan plane to save computational cost. All wind-tunnel walls (i.e., top, bottom, and side walls) are treated as viscous (no-slip) walls. Because the main objective of this numerical study is to examine the influence of wind-tunnel side walls on the flow characteristics in the midspan region of the airfoil, corresponding 2-D computations (i.e., using the same tunnel height, length, and the airfoil location but without the side wall) are also performed and compared with the midspan solution of the 3-D computations.

The freestream conditions simulated in this study also follow the aforementioned wind-tunnel tests at NASA Langley Research Center: the Reynolds number is 0.49×10^6 (based on the freestream velocity U_∞ and the airfoil chord length c) and the freestream Mach number is 0.1.

III. Computational Details

Both 2-D and 3-D computations were performed using the Stanford University multiblock flow solver [20]. The code is based on a finite volume method, which spatially discretizes the compressible RANS, energy, and turbulence model equations with second-order accuracy. The working fluid (air) is assumed to be a perfect gas, and the viscosity is calculated from Sutherland's law.

For the computational mesh, 2-D and 3-D multiblock structured meshes were created and used; the 2-D mesh was created first and then the 3-D mesh was created by extending the 2-D mesh in the spanwise (z) direction. Figure 3 shows the 2-D mesh around and inside the CC airfoil model. Note that the geometry of the jet plenum in this numerical study was simplified from the original model shown in Fig. 1 (the upstream chamber was eliminated and curved corners were replaced with sharp ones) so that the mesh was easily created with structured grids. The mesh inside the plenum consists of five blocks of structured grids (with 2500 grid points for the 2-D case), whereas the mesh around the airfoil consists of 23 blocks of structured grids (with 122,100 grid points for the 2-D case, where 400 grid points are on the Coanda surface and 500 grid points are on the other part of the airfoil surface). The grid resolution in the wall-normal direction is $\Delta y^+ < 1$ for most of the airfoil surface (except for the region very close to the jet exit). For the 3-D case, 80 grid points are nonequidistantly located in the spanwise (z) direction (with more grid points are clustered near the side wall than in the midspan region) while keeping the same 2-D mesh in the (x, y) plane, resulting in about 10 million grid points in total.

As concerns the boundary conditions, viscous (no-slip) conditions were applied at the airfoil surface and the wind-tunnel walls, whereas the midspan plane in the 3-D case was treated as a plane of symmetry, as noted in the previous section (cf. Fig. 2). For the outlet boundary of the wind-tunnel section, a constant static pressure (101325 Pa) was given. For the inlet boundary of the wind-tunnel section, however, the dynamic pressure was adjusted (keeping a constant total temperature of 297 K) so that the freestream Reynolds number and the Mach number matched the experimental values (0.49×10^6 and 0.1, respectively) for each simulation case. Note that the inlet flow has zero boundary-layer thickness on the wind-tunnel walls in this study, assuming that the incoming boundary layers were sucked at the inlet of the wind tunnel. Also assumed was a low freestream turbulence level at the inlet; an eddy viscosity ratio (the ratio of turbulent eddy viscosity to laminar viscosity) of 0.01 and a turbulence intensity of

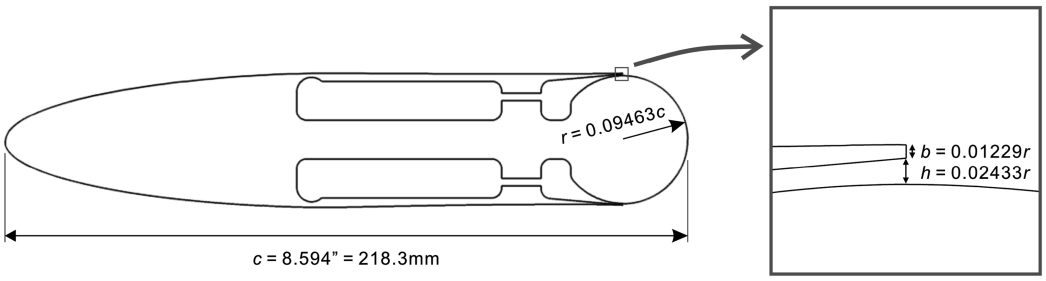

Fig. 1 Geometry of the CC airfoil model.

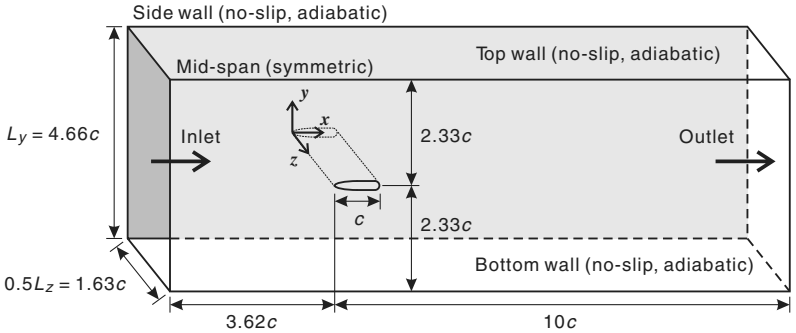

Fig. 2 Computational domain and boundary conditions (for the 3-D cases).

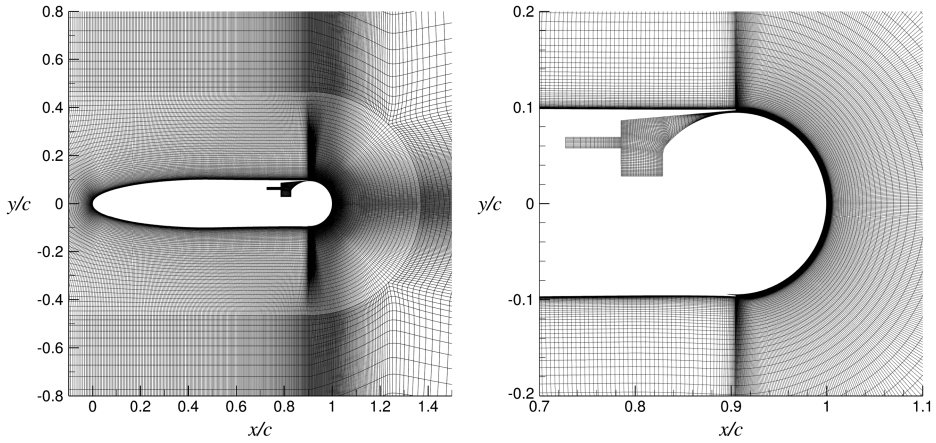

Fig. 3 Computational mesh: a) around the airfoil model, and b) around the Coanda trailing edge.

0.1% were given for the cases using the SST model, and the same eddy viscosity ratio was given for the cases using the SA model. For the inlet boundary of the Coanda jet plenum, again the dynamic pressure was adjusted (keeping a constant total temperature of 297 K) so as to obtain four different jet-mass-flow-rate conditions investigated in this study (see Table 1 in the next section).

All 2-D and 3-D computations were first performed in steady-state mode to quickly obtain approximate solutions of the flow (these steady-state computations did not converge to steady solutions). The approximate solutions were then used as initial conditions for time-accurate computations, which eventually converged to steady solutions when using a small enough time step of $\Delta t = 1.6 \times 10^{-5}$ s ($U_\infty \Delta t/c = 2.5 \times 10^{-3}$) in this study. A larger time step of $\Delta t = 3.2 \times 10^{-5}$ s was also tested for comparison and was found to give the same steady solutions as the smaller time step (the difference in the lift coefficient of the airfoil calculated was less than 0.1%) but an even larger time step of $\Delta t = 6.4 \times 10^{-5}$ s was found not to be small enough for the computations to converge. For the time-accurate computations, a second-order fully implicit scheme was used for the time integration.

IV. Results and Discussion

A. Jet Blowing Conditions

Table 1 summarizes the four jet-blowing conditions investigated in this study, together with some key results that will be described later in detail. Note that this table compares three different solutions (namely 3-D whole, 3-D midspan, and 2-D) for each turbulence model at each jet blowing condition: 3-D whole means the solutions for the whole computational domain (obtained from 3-D simulations), whereas 3-D midspan means the solutions at the midspan plane (obtained from the same 3-D simulations). Hence comparisons between 3-D whole and 3-D midspan reflect the three-dimensionality in the 3-D simulations, whereas comparisons between 3-D midspan and 2-D indicate sidewall effects on the solutions at the midspan plane. Here the jet momentum coefficient C_μ is defined as follows:

$$C_\mu = \frac{\dot{m}_j U_j}{\frac{1}{2}\rho_\infty U_\infty^2 c} \tag{1}$$

where $\dot{m}_j$ is the jet mass flow rate per unit span, U_j is the bulk (i.e., spatially averaged) jet velocity at the jet exit, and ρ_∞ is the freestream

Table 1 Computational conditions and key results

Jet blowing condition	Turbulence model	Dimension	Jet mass flow rate per unit span, kg/s-m	C_μ	C_L	Tunnel mass flux ratio (upper/lower)
Lowest ($C_\mu \approx 0.05$)	SST	3-D (whole)	0.0670	0.0471	1.57	1.91
		3-D (midspan)	0.0673	0.0475	1.61	1.92
		2-D	0.0672	0.0473	1.68	1.94
	SA	3-D (whole)	0.0669	0.0471	1.77	1.97
		3-D (midspan)	0.0672	0.0475	1.82	1.97
		2-D	0.0671	0.0474	1.87	2.00
Medium-low ($C_\mu \approx 0.08$)	SST	3-D (whole)	0.0887	0.0824	2.68	2.12
		3-D (midspan)	0.0890	0.0832	2.77	2.13
		2-D	0.0887	0.0828	2.88	2.16
	SA	3-D (whole)	0.0884	0.0825	3.00	2.20
		3-D (midspan)	0.0888	0.0833	3.09	2.20
		2-D	0.0885	0.0828	3.17	2.24
Medium-high ($C_\mu \approx 0.11$)	SST	3-D (whole)	0.1040	0.1133	3.61	2.36
		3-D (midspan)	0.1043	0.1142	3.73	2.36
		2-D	0.1040	0.1136	3.86	2.43
	SA	3-D (whole)	0.1035	0.1132	3.94	2.45
		3-D (midspan)	0.1039	0.1143	4.07	2.46
		2-D	0.1035	0.1137	4.21	2.52
Highest ($C_\mu \approx 0.14$)	SST	3-D (whole)	0.1161	0.1408	4.39	2.60
		3-D (midspan)	0.1163	0.1419	4.56	2.60
		2-D	0.1161	0.1414	4.74	2.70
	SA	3-D (whole)	0.1153	0.1405	4.70	2.70
		3-D (midspan)	0.1157	0.1418	4.87	2.71
		2-D	0.1154	0.1412	5.09	2.81

air density. Note that, in experimental studies, the bulk jet velocity U_j is usually estimated from readily available experimental quantities (i.e., total temperature and pressure of the plenum gas) to calculate C_μ [1]. In the present study, however, U_j is directly obtained from the flow solutions at the jet exit. Also note that the above definition of C_μ in this study can be used for both 2-D and 3-D solutions; for 3-D solutions, $\dot{m}_j$ is calculated as the 3-D jet mass flow rate divided by the spanwise length of the domain.

Figure 4 shows the relationship between $\dot{m}_j$ and C_μ for all 2-D and 3-D solutions obtained in this study. The very small difference between 3-D whole and 3-D midspan indicates that the jet flow is quasi-2-D at the jet exit (which will be shown later), whereas that between 3-D midspan and 2-D (and also between SA and SST cases) shows that the jet blowing condition (i.e., the dynamic pressure at the inlet of the jet plenum) was adjusted properly in this study. The differences in C_μ (at each jet-blowing level) are all less than 1%, which is small enough that meaningful comparisons between the 2-D and 3-D simulations can be made to investigate the mechanisms of wind-tunnel sidewall effects in the following subsections.

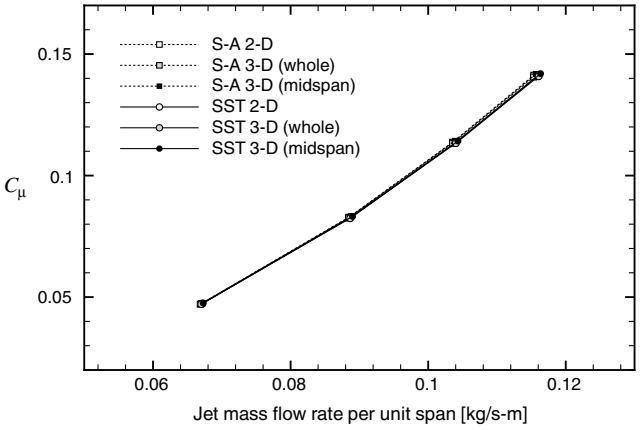

Fig. 4 Jet momentum coefficient versus jet mass flow rate.

B. Three-Dimensional Flow Patterns Around the Airfoil

Figure 5 describes 3-D flow patterns behind the CC airfoil model (calculated using the SST model, at $C_\mu \approx 0.14$). Figure 5a shows streamlines on the midspan plane together with the contours of nondimensional spanwise velocity (U_z/U_∞) at five different streamwise locations, whereas Fig. 5b shows streamlines starting from the Coanda jet exit together with the contours of the magnitude of nondimensional streamwise vorticity ($|\Omega_x|c/U_\infty$) at four different streamwise locations, for the same 3-D solution. Note that these figures include mirror images to show the whole wind-tunnel test section for visual purposes; the actual 3-D simulations were performed only for half of the test section in the spanwise direction in this study as already mentioned. The figures show that the quasi-2-D jet sheet separates from the Coanda trailing edge downward (the jet separation location is about 104 deg from the upper jet exit in this case) and then changes the flow direction toward the wind-tunnel streamwise direction. The spanwise ends of this jet sheet, however, three-dimensionally roll up on the side walls of the wind tunnel (cf. Fig. 6) to form large streamwise vortices behind the airfoil model, in such a way that the two counter-rotating streamwise vortices create downwash at the midspan plane. Of particular importance is that these two streamwise vortices are lifted up due to their own induced velocity. Although not shown here, similar 3-D flow patterns were observed at lower jet-blowing cases as well, with the size of the streamwise vortices getting smaller as the jet-blowing rate decreased.

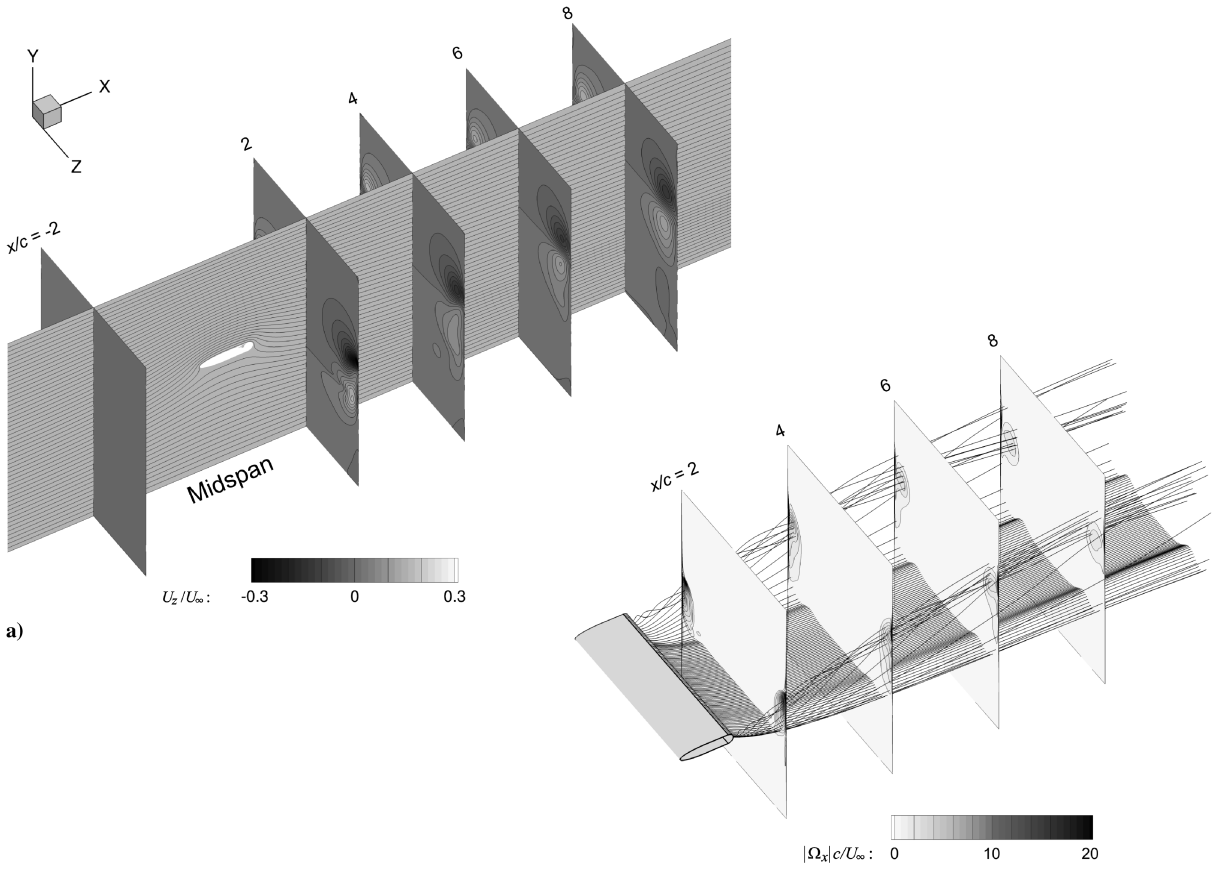

Fig. 5 Three-dimensional flow patterns behind the CC airfoil model (SST model, $C_\mu \approx 0.14$): a) streamlines on the midspan plane and contours of spanwise velocity, and b) streamlines starting from the jet exit and contours of the magnitude of streamwise vorticity.

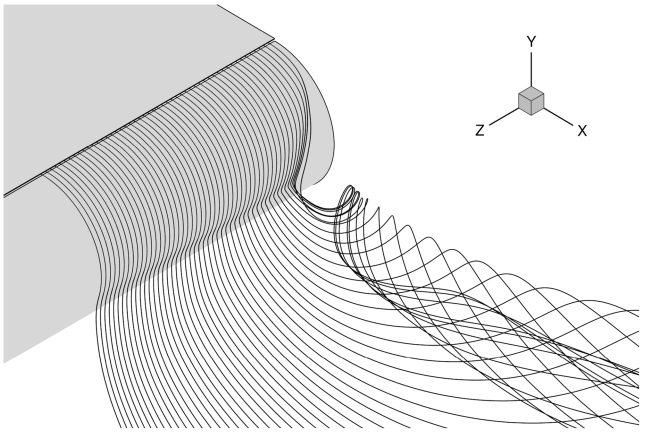

Fig. 6 Streamlines starting from the jet exit near the sidewall (SST model, $C_\mu \approx 0.14$).

Figure 7 shows in-plane streamlines at four different spanwise locations (0.1, 2, 5, and 50% span measured from the side wall) for the same 3-D solution as Figs. 5 and 6. Note that these streamlines are based on the in-plane velocity field (U_x, U_y) at each spanwise location. It can be seen that the front stagnation location of the flow is away from the airfoil surface at the 0.1% spanwise location (about 0.7 mm away from the side wall, representing surface oil flow visualization) due to the formation of horseshoe vortices around the junctions of the airfoil model and the side walls (Fig. 7a). At the 2% spanwise location, however, the front stagnation location of the flow is found on the airfoil surface (Fig. 7b), showing that the spanwise size of the horseshoe vortices near the leading edge is very small compared with that of the streamwise vortices behind the airfoil. This suggests that the three dimensionality of the flow around the CC airfoil is mainly due to the formation of the two streamwise vortices behind the airfoil.

C. Sidewall Effects on the Coanda Jet Flow

Although the quantitative accuracy of these 3-D flow patterns is unknown since there are no experimental data yet available to compare to, it is still of great interest to see how large the influence of the two streamwise vortices behind the airfoil is on the Coanda jet flow over the rounded trailing-edge surface. Figure 8 shows nondimensional tangential velocity (U_θ/U_∞) profiles around the Coanda trailing-edge surface at $\theta = 0$, 30, 60, and 90 deg (calculated using the SST model, at $C_\mu \approx 0.05$, 0.08, 0.11, and 0.14). Note that θ is the angle from the upper jet exit. The three different line types show the results of the 3-D simulations at three different spanwise locations (10, 30, and 50% span), whereas the symbols show the results of the 2-D simulations. It can be seen that the velocity profiles at the 30 and 50% spanwise locations are almost identical at all four tangential θ locations at all four jet-blowing conditions. The velocity profiles at the 10% spanwise location also look similar to the profiles at the 30 and 50% span except for the region after the flow separation (cf. Figs. 8a and 8b), showing that the Coanda jet flow is quasi-2-D for a fairly wide region around the 50% span (midspan) plane before the separation of the flow from the Coanda surface. Also of interest is the very close agreement between the profiles at the midspan of the 3-D simulations and the profiles from the 2-D simulations, showing that the influence of the wind-tunnel side walls is negligible on the Coanda jet flow around the trailing-edge surface at the midspan plane.

Figure 9 compares the jet separation angles between the 2-D simulations and the midspan solutions of the 3-D simulations. Note that the results calculated using the SA model are also plotted here for

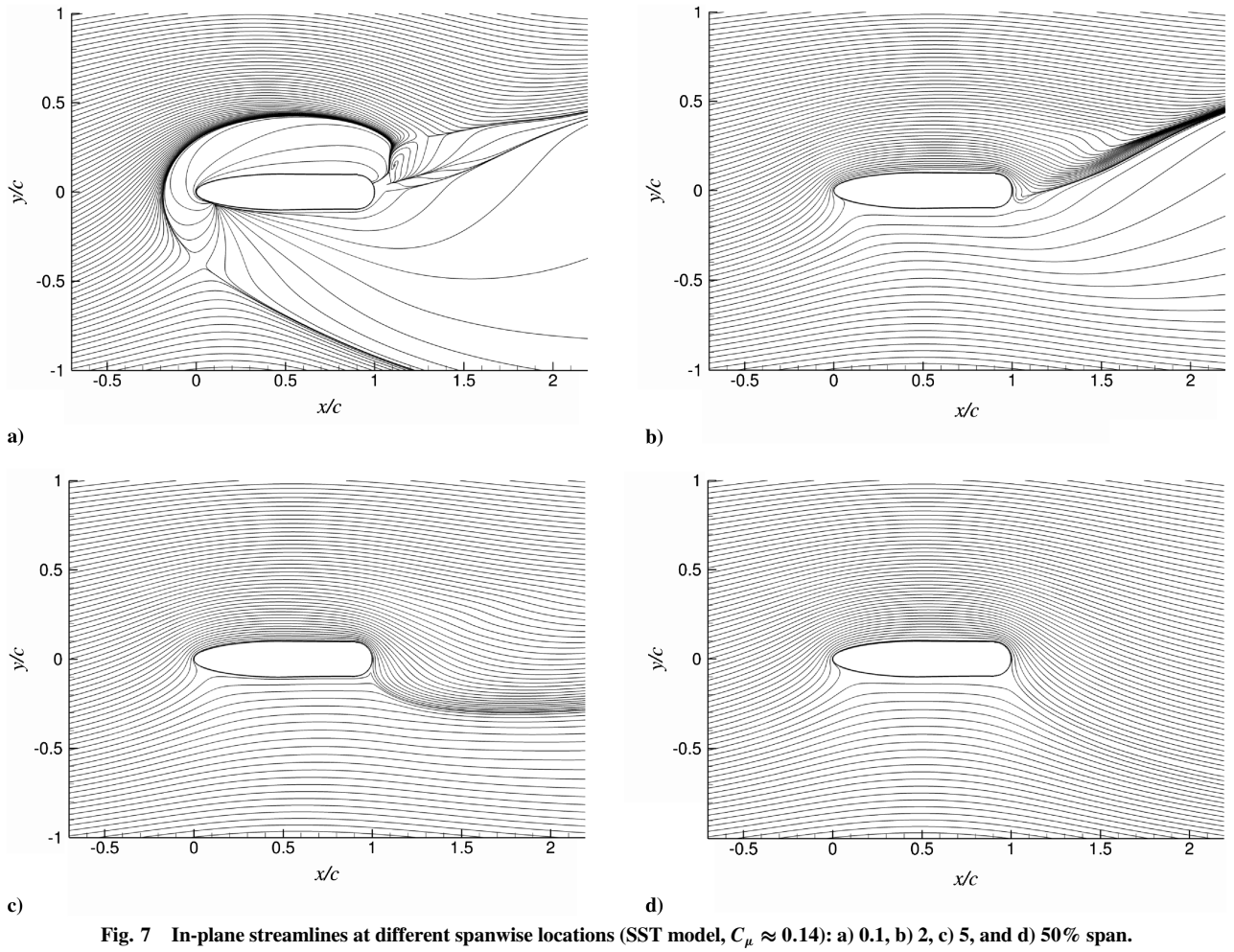

Fig. 7 In-plane streamlines at different spanwise locations (SST model, $C_\mu \approx 0.14$): a) 0.1, b) 2, c) 5, and d) 50% span.

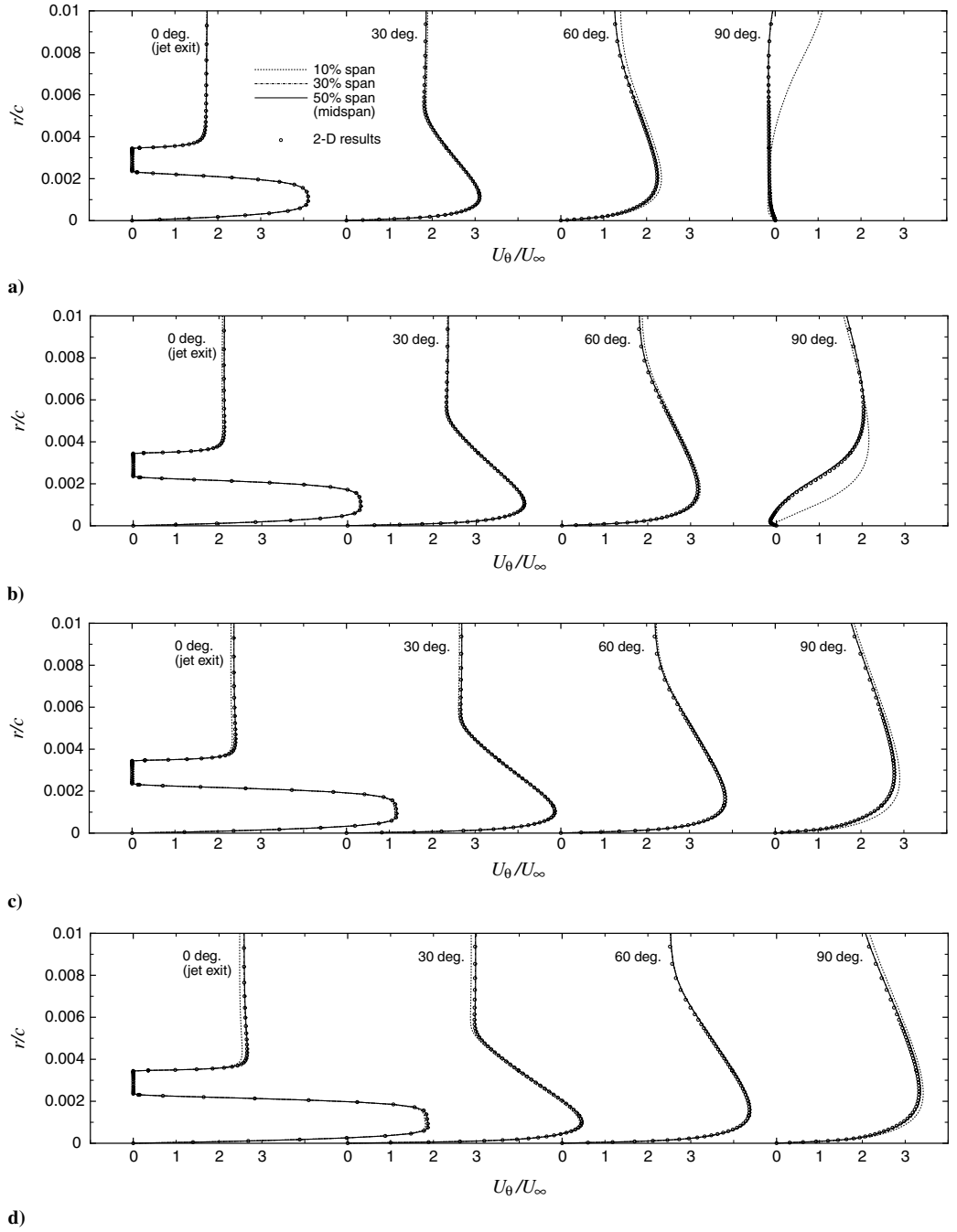

Fig. 8 Tangential velocity profiles around the Coanda trailing-edge SST model: a) $C_\mu \approx 0.05$, b) $C_\mu \approx 0.08$, c) $C_\mu \approx 0.11$, and d) $C_\mu \approx 0.14$.

comparison. It can be seen that the differences between 2-D and 3-D midspan are very small even at higher jet-blowing cases, although the SA model predicted the separation angle somewhat larger than the SST model at all jet-blowing cases. This again shows that the influence of the wind-tunnel side walls is very small on the Coanda jet flow at the midspan plane.

D. Sidewall Effects on the Flow Around the Airfoil

Figure 10 shows nondimensional streamwise velocity (U_x/U_∞) profiles across the wind-tunnel height at $x/c = -1, -0.5, 0, 0.5$, and 1 (calculated using the SST model, at $C_\mu \approx 0.14$). Note that the results of the 3-D simulation at three different spanwise locations (10, 30, and 50% span) as well as the results of the 2-D simulation are plotted in this figure, similar to Fig. 8. It can be seen that the velocity profiles at the 30 and 50% spanwise locations are almost identical at all five streamwise locations, showing that the wind-tunnel stream around the airfoil model is also quasi-2-D for a wide region around

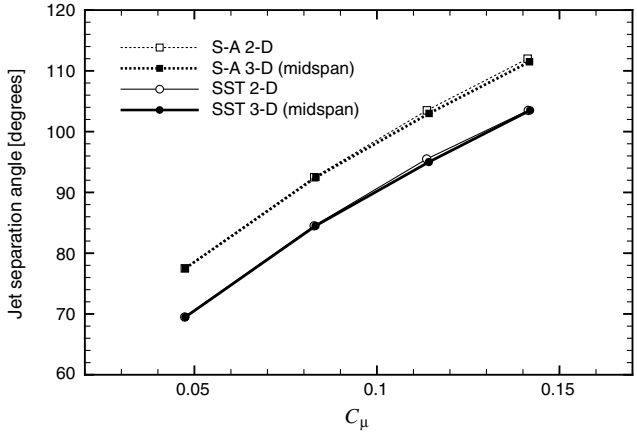

Fig. 9 Jet separation angle versus jet momentum coefficient.

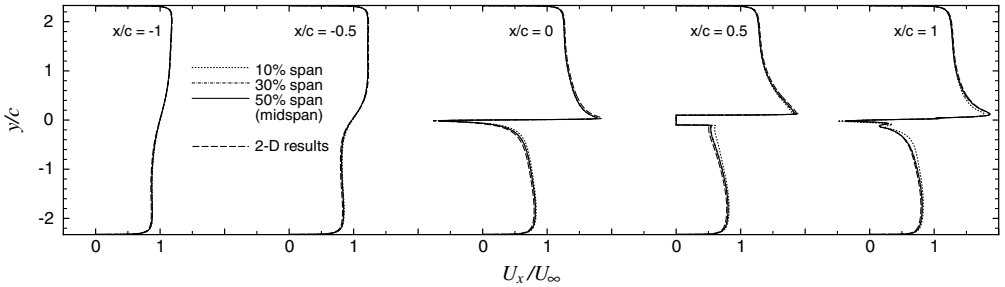

Fig. 10 Streamwise velocity profiles across the wind-tunnel height (SST model, $C_\mu \approx 0.14$).

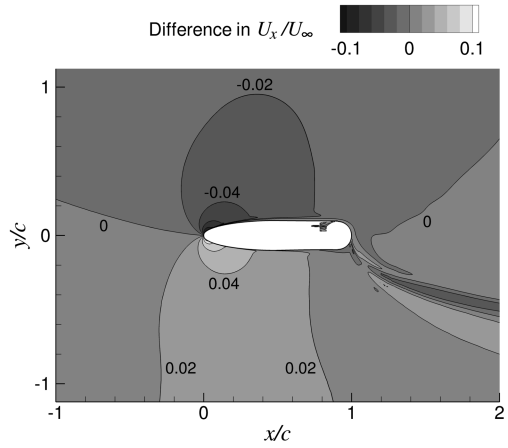

Fig. 11 Contours of the difference in U_x/U_∞ between the 2-D simulation and the midspan solution of the 3-D simulation (SST model, $C_\mu \approx 0.14$).

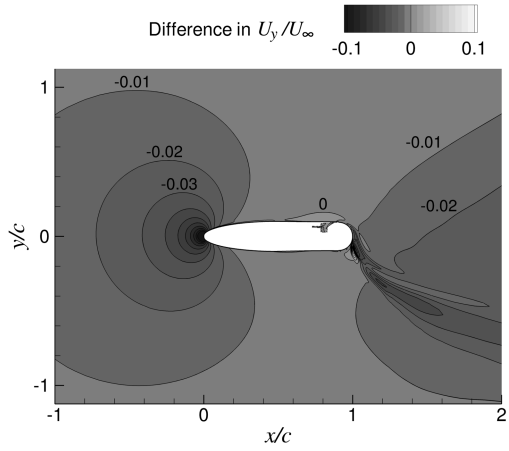

Fig. 12 Contours of the difference in U_y/U_∞ between the 2-D simulation and the midspan solution of the 3-D simulation (SST model,

the 50% span (midspan) plane upstream of the Coanda trailing-edge region. Of more significance, however, are the differences between the 2-D simulation and the midspan solution of the 3-D simulation: the midspan flow in the 3-D simulation is slightly decelerated above the airfoil model ($y/c > 0$) and is slightly accelerated below the airfoil model ($y/c < 0$) compared with the 2-D simulation. This can be seen more clearly in Fig. 11, which shows the contours of the difference in U_x/U_∞ around the airfoil between the 2-D simulation and the midspan solution of the 3-D simulation. Note that the differences plotted here were calculated by subtracting 2-D from 3-D midspan so that the contours show how much the midspan flow in the 3-D simulation is accelerated (positive differences in U_x/U_∞) or decelerated (negative differences in U_x/U_∞) compared with the 2-D simulation. Similarly, Fig. 12 shows the contours of the difference in U_y/U_∞ around the airfoil between the 2-D simulation and the midspan solution of the 3-D simulation. It can be seen that the effects of the side walls in the 3-D simulation result in a downwash in the midspan region not only downstream of the airfoil but also upstream of the airfoil, compared with the 2-D simulation.

Figure 13 shows the profiles of the pressure coefficient C_p on the airfoil model (calculated using the SST model, at $C_\mu \approx 0.14$). Again the profiles at the 30 and 50% spanwise locations are almost identical, indicating the quasi-two-dimensionality of the flow around the midspan plane. Comparing the 2-D simulation and the midspan solution of the 3-D simulation, however, it can be seen that the 3-D simulation predicts higher pressure (weaker suction) on the upper side of the airfoil especially near the leading edge (since the flow around there is slower than that in the 2-D simulation, as previously shown in Figs. 10 and 11). This difference in pressure around the leading edge mainly contributes to the difference in the lift and drag coefficients (C_L and C_D) of the airfoil. Figures 14 and 15 compare the calculated C_L and C_D between the 2-D simulations and the midspan solutions of the 3-D simulations for all four jet-blowing cases. Note that the results calculated using the SA model are also plotted here for comparison. It is clearly seen that the midspan solutions of the 3-D simulations give smaller C_L and larger C_D values than the corresponding 2-D simulations, and the difference between them (showing the sidewall effects) increases as the jet-blowing rate increases.

Another useful parameter to quantify the sidewall effects on the flow around the airfoil is the ratio of mass flux above and below the airfoil, since the airfoil model in this study spans the entire

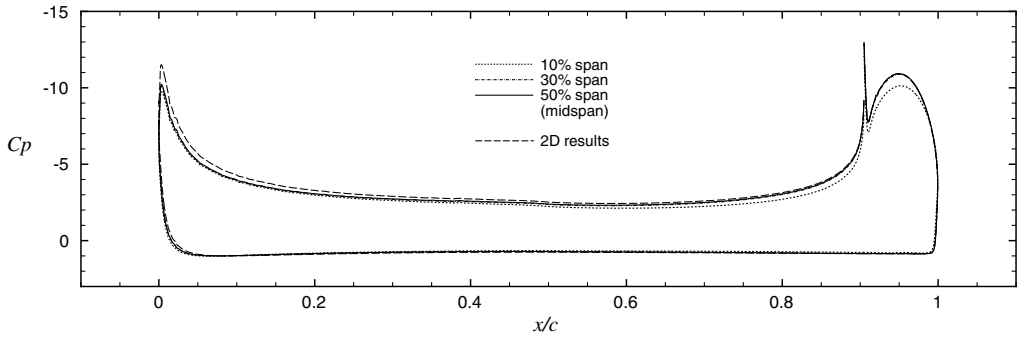

Fig. 13 Pressure distributions on the CC airfoil model (SST model, $C_\mu \approx 0.14$).

$C_\mu \approx 0.14$).

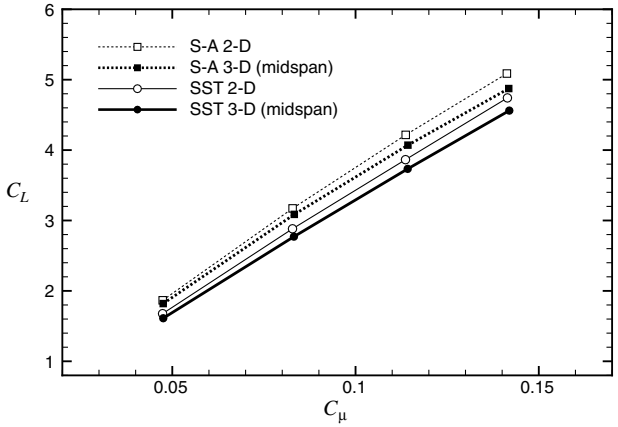

Fig. 14 Lift coefficient versus jet momentum coefficient.

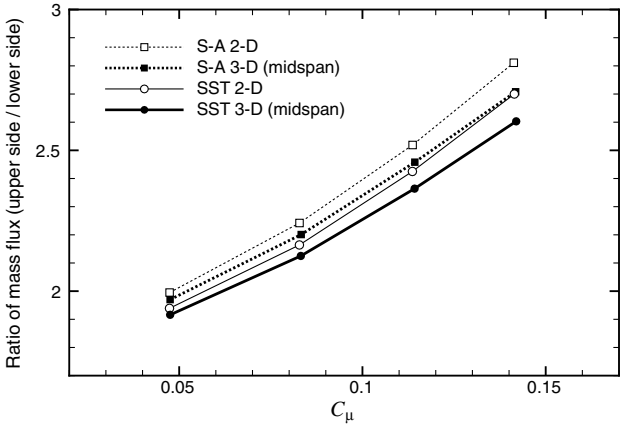

Fig. 16 The ratio of wind-tunnel mass flux (upper side of the airfoil divided by the lower side of the airfoil) versus jet momentum coefficient.

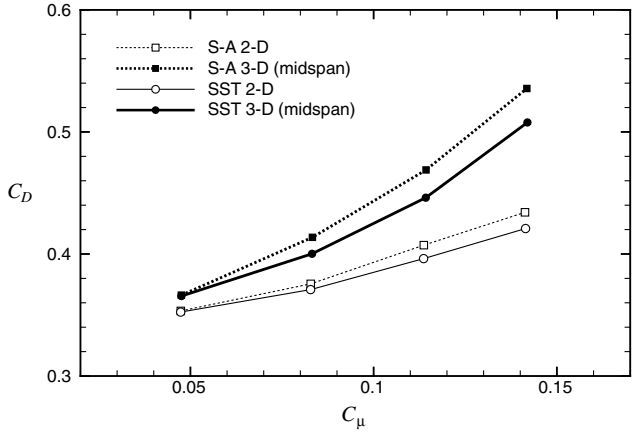

Fig. 15 Drag coefficient versus jet momentum coefficient.

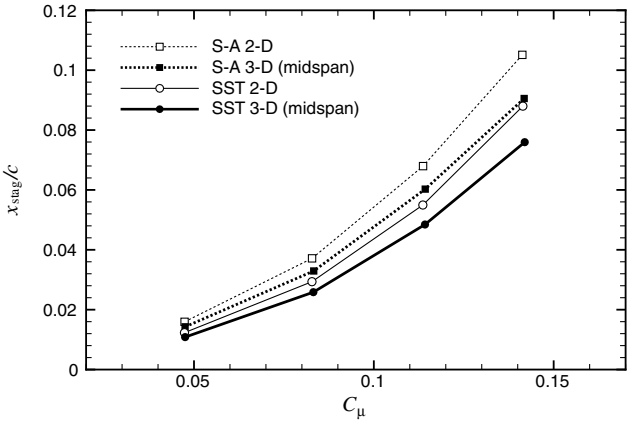

Fig. 17 Front stagnation location versus jet momentum coefficient.

wind-tunnel test section and thus divides it into the upper and lower passages. Figure 16 shows the calculated mass-flux ratio (the mass flux through the upper side divided by that through the lower side) for the 2-D simulations and the midspan solutions of the 3-D simulations. Note that the mass-flux ratio increases (i.e., more wind-tunnel stream goes through the upper side) as the jet-blowing rate increases. Comparing 2-D and 3-D midspan solutions, however, it can be seen that the wind-tunnel stream at the midspan plane in the 3-D simulations goes more through the lower side compared with that in the 2-D simulations, and again the difference between them (showing the sidewall effects) increases as the jet-blowing rate increases. Also of interest is the front stagnation location of the wind-tunnel stream on the airfoil surface, which reflects the mass-flux ratio above and below the airfoil. Figure 17 shows the nondimensionalized front stagnation location (x_{stag}/c) for the 2-D simulations and the midspan solutions of the 3-D simulations. Note that the stagnation location moves downstream along the lower surface of the airfoil as the jet-blowing rate increases and thus the circulation around the airfoil increases. Comparing 2-D and 3-D midspan solutions, however, it can be seen that the front stagnation location at the midspan plane in the 3-D simulations is more upstream on the lower surface of the airfoil (and thus more wind-tunnel stream goes through the lower side) compared with that in the 2-D simulations.

The key question here is why the wind-tunnel stream goes through the lower side more in the 3-D simulations than in the 2-D simulations. The most probable explanation is that the large streamwise vortices created behind the airfoil in the 3-D simulations entrain the wind-tunnel stream more from the lower side of the airfoil than from

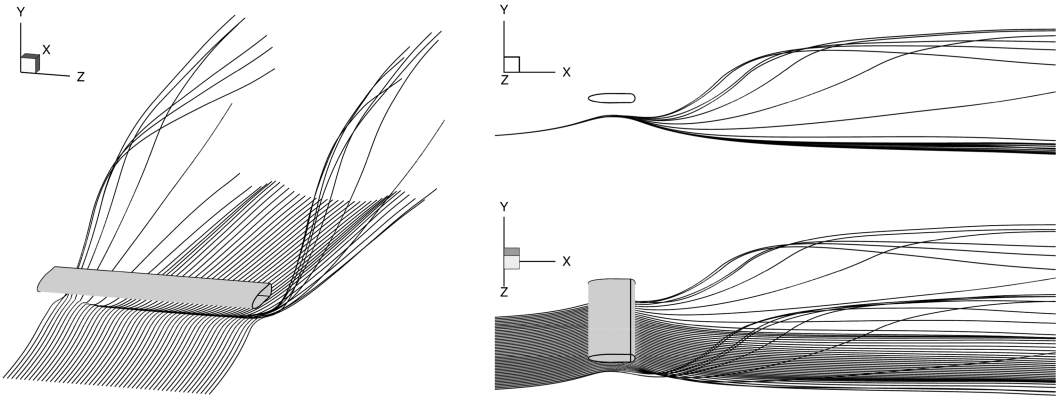

Fig. 18 Streamlines starting from $(x/c, y/c) = (-2, -0.8)$, illustrating the wind-tunnel stream that goes below the airfoil and then rolls up behind the airfoil (SST model, $C_\mu \approx 0.14$).

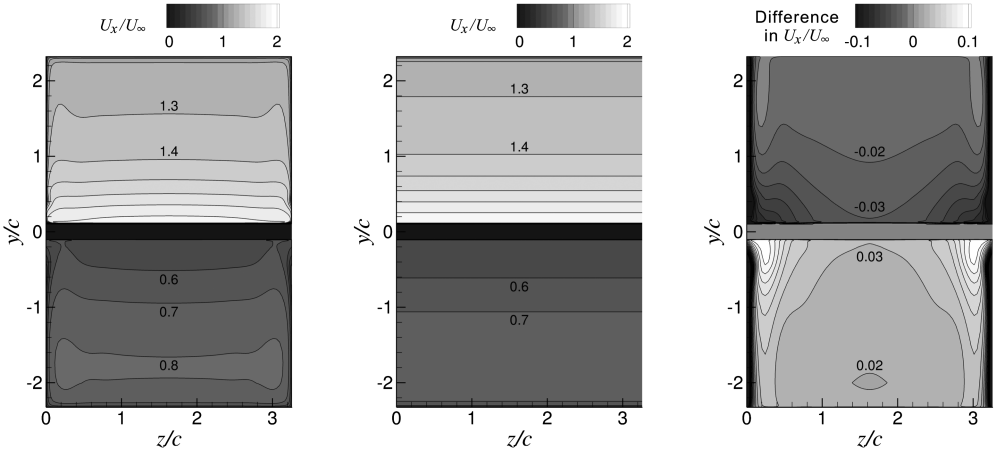

a) b) c)

Fig. 19 Contours of streamwise velocity at the midchord ($x/c = 0.5$) plane (SST model, $C_\mu \approx 0.14$): a) 3-D simulation, b) 2-D simulation, and c) difference between the 3-D and 2-D simulations.

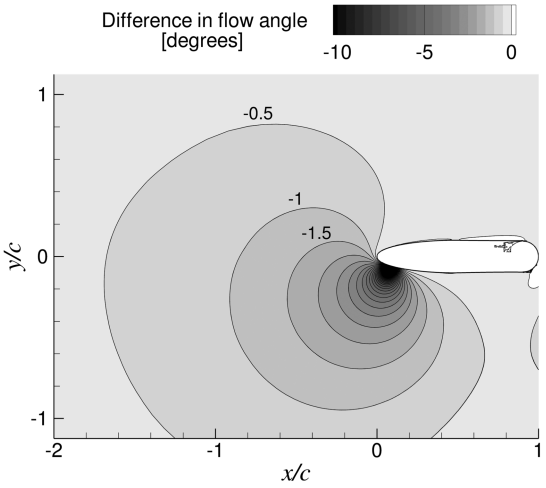

Fig. 20 Contours of the difference in local flow angle between the 2-D simulation and the midspan solution of the 3-D simulation (SST, $C_\mu \approx 0.14$).

the upper side of the airfoil. Figure 18 plots streamlines originating at $(x/c, y/c) = (-2, -0.8)$ to illustrate the wind-tunnel stream that goes below the airfoil (calculated using the SST model, at $C_\mu \approx 0.14$). Note that the three subfigures in Fig. 18 describe the same 3-D solution from three different points of view, for visualization purposes. It can be seen that the near-sidewall stream that goes below the airfoil is entrained by the large streamwise vortices and is lifted up behind the airfoil. The influence of this entrainment on the near-sidewall stream below the airfoil can be seen more clearly in Fig. 19, which shows the contours of nondimensional streamwise velocity (U_x/U_∞) at the midchord ($x/c = 0.5$) plane for the 3-D and 2-D simulations (Figs. 19a and 19b, respectively) and the contours of the differences between them (Fig. 19c, all calculated using the SST model, at $C_\mu \approx 0.14$). It can be seen that the flow is accelerated below the airfoil (and is decelerated above the airfoil) in the 3-D simulation compared with that in the 2-D simulations, and the peaks of the acceleration are located near the side walls.

Finally, Fig. 20 shows the contours of the difference in local flow angle between the 2-D simulation and the midspan solution of the 3-D simulation (calculated using the SST model, at $C_\mu \approx 0.14$). Note that the differences plotted here were calculated by subtracting the flow angle in 2-D from that in 3-D midspan. It can be seen that the flow angle around the leading edge at the midspan of the 3-D simulation is reduced (since the wind-tunnel stream goes more below the airfoil) compared with that in the 2-D simulation.

V. Conclusions

In this study, 2-D and 3-D compressible RANS simulations were performed on the flow around a basic CC airfoil model placed in a rectangular wind-tunnel test section to investigate the physical mechanisms of the wind-tunnel sidewall effects. The computations were conducted in a time-resolved manner with a small enough time step to eventually provide converged, steady RANS solutions. The SST turbulence model of Menter was mainly used but the SA model was also used for comparison. The two models were found to provide qualitatively similar solutions at all four jet-blowing conditions investigated, supporting the conjecture that the conclusions described below are not sensitive to the specific turbulence models used in the simulations.

The 3-D RANS solutions showed that the sidewall effects on the Coanda jet flow profiles over the trailing edge were very small: the jet flow was found to be quasi-2-D for a fairly wide region around the midspan plane before the separation of the flow from the Coanda surface. The spanwise ends of this quasi-2-D jet sheet having separated from the Coanda surface, however, rolled up on the side walls of the wind tunnel to form two large streamwise vortices downstream of the airfoil model (and they were lifted up further downstream due to their own induced velocity). Careful comparisons between the 2-D and 3-D RANS solutions then revealed that the wind-tunnel stream went through the lower side of the tunnel (below the airfoil) more in the 3-D cases than in the 2-D cases due to the entrainment and rolling-up by these streamwise vortices downstream. As a result, smaller lift and larger drag were produced at the midspan of the airfoil in the 3-D cases than in the 2-D cases.

These results obtained in this numerical study will be useful for understanding the qualitative effects of wind-tunnel side walls when comparing wind-tunnel experiments with high-fidelity numerical simulations such as LES, which cannot directly address the sidewall effects due to their huge computational cost. A possible next step towards a better comparison between such high-fidelity numerical simulations and wind-tunnel experiments might be to model the sidewall effects and build them into the numerical simulations. It should be reiterated, however, that the results obtained in the present RANS study were only qualitatively reliable. For such a modeling of sidewall effects for high-fidelity numerical simulations, better quantitative estimates of the sidewall effects need to be achieved beforehand (by using improved or empirically calibrated RANS simulations, or more reliable RANS-LES hybrid simulations), and this seems a challenging task.

Acknowledgments

The present work was supported by NASA's Fundamental Aeronautics Program (Subsonic Fixed Wing Project), and T. Nishino

has been supported by the NASA Postdoctoral Program administrated by Oak Ridge Associated Universities. The authors would like to thank S. Hahn of the Center for Turbulence Research at Stanford University for providing the computational code, G. Jones and B. Allan of NASA Langley Research Center for providing the airfoil geometry, and M. Rogers and N. Madavan of NASA Ames Research Center for many valuable discussions.

References

[1] Englar, R. J., "Circulation Control Pneumatic Aerodynamics: Blown Force and Moment Augmentation and Modification; Past, Present & Future," *Fluids 2000*, AIAA Paper 2000-2541, June 2000.

[2] Tennant, J. S., Johnson, W. S., and Krothapalli, A., "Rotating Cylinder for Circulation Control on an Airfoil," *Journal of Hydronautics*, Vol. 10, No. 3, 1976, pp. 102–105. doi:10.2514/3.48147

[3] Slomski, J. F., Gorski, J. J., Miller, R. W., and Marino, T. A., "Numerical Simulation of Circulation Control Airfoils as Affected by Different Turbulence Models," *40th AIAA Aerospace Sciences Meeting and Exhibit*, Reno, NV, AIAA Paper 2002-0851, Jan. 2002.

[4] Swanson, R. C., and Rumsey, C. L., "Numerical Issues for Circulation Control Calculations," *3rd AIAA Flow Control Conference*, San Francisco, CA, AIAA Paper 2006-3008, June 2006.

[5] Swanson, R. C., and Rumsey, C. L., "Computation of Circulation Control Airfoil Flows," *Computers and Fluids*, Vol. 38, No. 10, 2009, pp. 1925–1942. doi:10.1016/j.compfluid.2009.05.002

[6] McGowan, G., Rumsey, C., Swanson, R. C., and Hassan, H., "A Three-Dimensional Computational Study of a Circulation Control Wing," *3rd AIAA Flow Control Conference*, San Francisco, CA, AIAA Paper 2006-3677, June 2006.

[7] Slomski, J. F., Chang, P. A., and Arunajatesan, S., "Large Eddy Simulation of a Circulation Control Airfoil," *3rd AIAA Flow Control Conference*, San Francisco, CA, AIAA Paper 2006-3011, June 2006.

[8] Hahn, S., and Shariff, K., "Large-Eddy Simulation of Flow Around a Circulation Control Airfoil," *IPLC 2008: International Powered Lift Conference*, Royal Aeronautical Society, London, July 2008.

[9] Nishino, T., Hahn, S., and Shariff, K., "Calculation of the Turbulence Characteristics of Flow Around a Circulation Control Airfoil Using LES," *48th AIAA Aerospace Sciences Meeting Including the New Horizons Forum and Aerospace Exposition*, Orlando, FL, AIAA Paper 2010-0347, Jan. 2010.

[10] Nishino, T., Hahn, S., and Shariff, K., "LES of High-Reynolds-Number Coanda Flow Separating from a Rounded Trailing Edge of a Circulation Control Airfoil," *8th International ERCOFTAC Symposium on Engineering Turbulence Modelling and Measurements*, ERCOFTAC, Marseille, France, June 2010

[11] Wood, N. J., and Rogers, E. O., "An Estimation of the Wall Interference on a Two-Dimensional Circulation Control Airfoil," *14th Aerodynamic Testing Conference*, AIAA Paper 1986-0738, West Palm Beach, FL, March 1986.

[12] Novak, C. J., Cornelius, K. C., and Roads, R. K., "Experimental Investigations of the Circular Wall Jet on a Circulation Control Airfoil," *AIAA 25th Aerospace Sciences Meeting*, Reno, NV, AIAA Paper 1987-0155, Jan. 1987.

[13] Spalart, P. R., "Detached-Eddy Simulation," *Annual Review of Fluid Mechanics*, Vol. 41, No. 1, 2009, pp. 181–202. doi:10.1146/annurev.fluid.010908.165130

[14] Nishino, T., Roberts, G. T., and Zhang, X., "Unsteady RANS and Detached-Eddy Simulations of Flow Around a Circular Cylinder in Ground Effect," *Journal of Fluids and Structures*, Vol. 24, No. 1, 2008, pp. 18–33. doi:10.1016/j.jfluidstructs.2007.06.002

[15] Rogers, S. E., Roth, K., and Nash, S. M., "Validation of Computed High-Lift Flows with Significant Wind-Tunnel Effects," *AIAA Journal*, Vol. 39, No. 10, 2001, pp. 1884–1892. doi:10.2514/2.1203

[16] Spalart, P. R., and Allmaras, S. R., "A One-Equation Turbulence Model for Aerodynamic Flows," *La Recherche Aerospatiale: Bulletin Bimestriel de l'Office National d'Etudes et de Recherches Aerospatiales*, Vol. 1, 1994, pp. 5–21.

[17] Menter, F. R., "Two-Equation Eddy-Viscosity Turbulence Models for Engineering Applications," *AIAA Journal*, Vol. 32, No. 8, 1994, pp. 1598–1605. doi:10.2514/3.12149

[18] Englar, R. J., "Circulation Control Aerodynamics for Very Efficient High-Lift and Cruise Performance for Subsonic/Transonic Air Vehicles," Annual Progress Rept., Year 1, Georgia Tech Research Inst., Warner Robins, GA, 2007.

[19] Jones, G. S., Lin, J. C., Allan, B. G., Milholen, W. E., Rumsey, C. L., and Swanson, R. C., "Overview of CFD Validation Experiments for Circulation Control Applications at NASA," *IPLC 2008: International Powered Lift Conference*, Royal Aeronautical Society, London, July 2008.

[20] van der Weide, E., Kalitzin, G., Schlüter, J., and Alonso, J. J., "Unsteady Turbomachinery Computations Using Massively Parallel Platforms," *44th AIAA Aerospace Sciences Meeting and Exhibit*, Reno, NV, AIAA Paper 2006-421, Jan. 2006.

A. Naguib
Associate Editor